Journal of King Saud University - Science 36 (2024) 103525

HOSTED BY

Contents lists available at ScienceDirect

Journal of King Saud University - Science

journal homepage: www.sciencedirect.com

Oxidants-induced high levels of nitric oxide impair the antioxidative property of molybdenum nanoparticles in HUVE cells

Mohd Javed Akhtar [a,*], Maqusood Ahamed [a], Sudhir Kumar [b], Rashid Lateef [c], Zabn Alaizeri [d], Hisham Alhadlaq [d], Pavan Rajanahalli [e]

[a] King Abdullah Institute for Nanotechnology, King Saud University, Riyadh 11451, Saudi Arabia
[b] Department of Zoology, University of Lucknow, Lucknow 226007, Uttar Pradesh, India
[c] Department of Biotechnology, Era University, Lucknow-226003, Uttar Pradesh, India
[d] Department of Physics and Astronomy, College of Sciences, King Saud University, Riyadh, Saudi Arabia
[e] Department of Biology, University of Tampa, Tampa, FL 33569, USA

ARTICLE INFO

Keywords:
Oxidative stress
Nitric oxide
ROS
Cytoprotectant
Nanotechnology

ABSTRACT

In recent years, there has been significant interest in the biomedical potential of redox-active molybdenum nanoparticles (Mo NPs) due to their varied responses from oxidative to antioxidative. Our knowledge of the bio-response of Mo NPs in endothelial cells is lacking. We, therefore, are prompted to examine the biocompatibility of well-characterized Mo NPs in human endothelial (HUVE) cells and their potential antioxidative response against standard oxidants- *tert*-butyl hydroperoxide (t-BHP) and hydrogen peroxide (H_2O_2). The study found that Mo NPs were highly biocompatible in HUVE cells and enhanced cellular antioxidant glutathione (GSH), significantly protecting cells against exogenous oxidants. Moreover, Mo NPs significantly restored the loss of mitochondrial membrane potential (MMP) determined by the Rh123 probe. They decreased reactive oxygen species (ROS) levels as measured by DHE and DCFH-DA probes. In light of Mo involvement in the nitric oxide (NO) metabolism and dependency of HUVE cells on NO signaling, intracellular NO was determined using DAR-2 fluorescent dye and the Griess assay. NO was not produced significantly by Mo NPs alone or t-BHP or H_2O_2. However, NO generation was significantly high when HUVE cells were co-exposed with Mo NPs and exogenous oxidants. Although the exact mechanism is unclear to us, our study concludes that the enhanced generation of NO under the co-exposure of oxidants with Mo NPs can impair the potential antioxidative property of Mo NPs, especially in endothelial cells. The study also suggests that NO modulatory strategies can improve and broaden the antioxidative properties of Mo-based nanoparticles.

1. Introduction

Nanoparticles of molybdenum (Mo NPs) have gained significant attention in biomedical sciences due to their versatile properties (Ahmed et al., 2021). Mo NPs hold immense potential for various applications, including imaging, therapy, and drug delivery (Dhas et al., 2021; Eremin et al., 2018). Mo NPs can be used as contrast agents for MRI, as photothermal agents for photothermal therapy, as well as carriers that can encapsulate or conjugate various drugs to achieve controlled and targeted release of drugs (Dhas et al., 2021; Kashyap et al., 2022). Probably, the most exciting thing about Mo NPs to us as investigators is that Mo NPs possess intriguing properties that make them potential candidates for various applications, particularly as antioxidant and anti-inflammatory agents (Feng and Cao, 2016; Ni et al., 2018; Ren et al., 2022; Yang et al., 2019). Firstly, Mo NPs have been studied for their antioxidant properties (Khafaji et al., 2019; Ni et al., 2018). Oxidative stress, caused by an imbalance between free radicals and antioxidants in the body, is associated with various diseases such as cardiovascular disorders, cancer, and neurodegenerative conditions (Fridovich, 2003). Inflammation and cancer onsets are directly linked with the chronic occurrences of oxidative stress (Reuter et al., 2010). Therefore, antioxidants and ROS scavenging agents can be explored to manage inflammation and cancer risks. Mo-based NPs and nano-formulations have demonstrated the ability to scavenge free radicals and inhibit oxidative damage by neutralizing these harmful species (Ni et al., 2018). By reducing oxidative stress, Mo NPs could potentially contribute to

* Corresponding author at: King Abdullah Institute for Nanotechnology (KAIN), King Saud University, P.O. Box 2454, Riyadh 11451, Saudi Arabia.
E-mail address: mjakhtar@ksu.edu.sa (M. Javed Akhtar).

https://doi.org/10.1016/j.jksus.2024.103525
Received 1 October 2023; Received in revised form 4 November 2024; Accepted 5 November 2024
Available online 6 November 2024

preventing or managing such diseases. However, Mo NPs have shown contradictory effects on inflammation (Han et al., 2022; Zapór et al., 2022). Inflammation is significant in numerous chronic conditions, including arthritis, cardiovascular diseases, and inflammatory bowel disease. Studies have indicated that Mo NPs possess anti-inflammatory activities by modulating pro-inflammatory mediators and cytokines, thus reducing the inflammatory response (Han et al., 2022). Some of the prominent avenues of exhibiting antioxidant and anti-inflammatory properties include quick replenishment of ubiquitous antioxidant cellular GSH and mimicking the enzyme-like activities of several antioxidant enzymes such as peroxidases and superoxidases (Dhas et al., 2021; Kashyap et al., 2022). Moreover, Mo NPs have shown excellent reducing potential by converting yellow MTT to blue formazan under a physiological aqueous solution. The ROS scavenging and antioxidant capacity of Mo NPs suggest their potential in developing therapeutics for combating oxidative stress-mediated diseases such as aging, inflammation, and cancer. However, it is essential to note that further research is needed to fully understand the mechanisms by which Mo NPs exert their antioxidant and anti-inflammatory effects and the mechanisms that might limit their potential uses. Harnessing the advantages of Mo NPs could potentially lead to improved treatment strategies for oxidative stress-related diseases and inflammatory conditions.

We investigated the potential biocompatibility and antioxidative/oxidative mechanism of Mo NPs in human umbilical vein endothelial cells (HUVECs) followed by NO modulation as Mo is part of many enzymes that deal with NO metabolism in mammalian cells (Valko et al., 2016). To our knowledge, this is novel research as the oxidative stress-modulating potential of Mo NPs has not been tested on HUVE cells before. To begin with, we tested HUVE cells for their tolerance to different Mo NPs concentrations utilizing MTT bioassay. We measured cellular GSH and mitochondrial membrane potential to assess the potential oxidative-modulating capacity of Mo NPs against known oxidative inducers: *tert*-butyl hydroperoxide (t-BHP) and hydrogen peroxide (H_2O_2). In light of Mo involvement in the NO metabolism and dependency of HUVE cells on NO signaling for crucial functions (Valko et al., 2016), evaluating NO levels in the context of Mo NPs exposure becomes vital. NO is a mildly reacting signaling molecule that can produce oxidative and antioxidative effects (Farah et al., 2018). This dual role of NO depends on its concentration, duration, and cellular context effects (Farah et al., 2018). In this study, we measured NO levels using DAR-2 fluorescent dye and the Griess assay. As discussed below, this suggests that Mo NPs may trigger high NO under oxidant exposure. NO can be a mechanism limiting the antioxidative potential of Mo NPs, especially in endothelial cells that perform crucial functions dependent on NO signaling.

2. Materials and methods

2.1. Chemicals and reagents

The following reagents were obtained from Invitrogen Co. (Carlsbad, CA, USA): Fetal bovine serum, penicillin–streptomycin, and CalceinAM. The rest of the chemicals, including DMEM F-12, MTT [3-(4,5-dimethyl thiazol-2-yl)-2,5-diphenyl tetrazolium bromide], NADH, pyruvic acid, perchloric acid, DCFH-DA, Rh123, DAR-2, GSH, o-phthalaldehyde (OPT), hank's balanced salt solution (HBSS) and Bradford reagent were obtained from Sigma–Aldrich. Ultrapure water was prepared from a Milli-Q system (Millipore, Bedford, MA, USA).

2.2. Procurement and Characterization of Mo NPs

The Mo NPs were acquired from Sigma-Aldrich, a reputable supplier. According to the information, these NPs were of high purity, with a 99.8 % composition, while containing trace amounts of other metals. The NPs were obtained in a powdered form, exhibiting a blackish color. To determine the actual size of the NPs, transmission electron microscopy (JEM-2100F, JEOL Inc., Akishima, Japan) was employed, operating at an accelerating voltage of 200 kV. Additionally, scanning electron microscopy (JSM-7600F, JEOL Inc., Akishima, Japan) was utilized to ascertain the shape of the NPs, with an accelerating voltage of 5 kV. The purity and chemical composition of the NPs were estimated using EDS analysis.

2.3. Surface adsorption analysis

As described in a previous article, the interaction of NPs with BSA proteins, a relevant biological protein, was assessed by BSA adsorption on Mo NPs (Akhtar et al., 2020). NPs at different concentrations were incubated with 0.5 mg/mL of BSA in phosphate buffer saline for 24 h with cycles of gentle shaking. Then, the mixtures were centrifuged at 12,000 × g for 10 min to pellet down NPs with adsorbed BSA. The supernatants were mixed with Bradford reagent, and the absorbance was read at 595 nm. The amount of BSA adsorbed on NPs was calculated from the decrease in the absorbance of supernatant containing unadsorbed free BSA. A higher decrease in absorbance indicated more BSA adsorbed on NPs and vice-versa.

2.4. Cell culture and treatments with NPs and oxidants

HUVECs (ATCC, Manassas, VA, USA) were cultured in DMEM-F12 media complemented with 10 % FBS, endothelial growth supplement (CADMEC, Cell Applications, Inc, San Diego, CA, USA), and 100 U/ml penicillin and 100 µg/mL streptomycin. The cells were incubated at 37 °C and 5 % CO_2 and passaged every 3–4 days. Mo NPs were sonicated in culture media for 5 min (UltrasonicCleaner-8891, Cole-Parmer, 625 Bunker Court Vernon Hills, IL USA) and diluted to the desired concentration in sterile tubes. Cells were exposed to NPs and oxidants 24 h after seeding. Control groups were untreated. IC50 of each oxidant was determined before co-exposure experiments.

2.5. MTT bioassay

In this study, the MTT assay was employed to evaluate cell viability, utilizing the methodology outlined by Mosmann (1983) with slight modifications. Initially, an approximate quantity of 1×10^4 HUVECs (human umbilical vein endothelial cells) was plated in a 96-well plate, possessing a smooth and even base. The cells were exposed to both NPs and oxidants on the subsequent day. Later, the MTT assay was conducted by measuring the absorbance at 570 nm, derived from a transparent supernatant devoid of NPs, after centrifuging the plate. Cell viability was expressed as a percentage relative to the control cells, with 100 % representing full viability in the control group.

2.6. CalceinAM assay

One of the techniques used to assess cell viability is the imaging of cells loaded with CalceinAM. This fluorescent dye produces bright green fluorescence in healthy cells but weaker green fluorescence in damaged ones or lacking in dead cells (Neri et al., 2001). This method allows the visualization of viable cells under a fluorescence microscope and the quantification of cell viability by measuring the fluorescence intensity, as briefed in our previous reports (Akhtar et al., 2023, 2021). Fluorescence in control cells is proof of 100 % cell viability. The advantages of this technique include its high sensitivity, specificity, and direct observation method.

2.7. Intracellular GSH assay

We measured the GSH content in cells using the method of Hissin and Hilf (1976). We washed the cells, scraped them off, and rewashed them in PBS. We lysed the cells in 0.1 % deoxycholic acid and 0.1 % sucrose solution for two h with three freeze–thaw cycles and spun them at

10,000 × g for 10 min at 4 °C. We precipitated the supernatant with 1 % perchloric acid and spun it at 10,000 × g for 5 min at 4 °C. We mixed 20 µL of the protein precipitate with 160 µL of phosphate–EDTA buffer (0.1 M, pH 8.3) and 20 µL of OPT (1 mg/mL in methanol) in a black 96 well plate. We incubated the plate for 2.5 h at room temperature in the dark and read the fluorescence at 460 nm (Biotek Synergy HT) with GSH standards. We estimated the protein from the unprecipitated supernatant and expressed the data as GSH nmol/mg protein.

2.8. Determination of ROS

To evaluate intracellular reactive oxygen species (ROS) production, we employed the fluorescent probe DCFH-DA which broadly measures H_2O_2 as introduced by Wang and Joseph (1999). After exposing the cells to NPs as described in the MTT assay, the medium was removed, and each well was treated with 100 µL of 50 µM DCFH-DA in Hank's Balanced Salt Solution (HBSS). The plates were then incubated for 45 min, allowing the DCFH-DA probe to penetrate the cells. Subsequently, the wells were washed twice with cold Phosphate Buffered Saline (PBS) to eliminate excess dye. The researchers measured the fluorescence emitted by the DCF at an emission wavelength of 528 nm using a plate reader (Synergy HT, Bio-Tek, Winooski, Vermont, USA). Hydroethidine (DHE) was employed to measure superoxide radical ($O_2^{\bullet-}$) by microscopy under live-cell settings, as briefed in a published article (Akhtar et al., 2022).

2.9. Mitochondrial membrane potential determination by Rh123 probe

Rhodamine 123 (Rh123) is a widely used fluorescent dye that is an excellent tool for studying MMP (Baracca et al., 2003; Johnson et al., 1980). In this assay, Rh123 was added to the cells in a 12-well plate at a final concentration of 5 µM and incubated with Rh123 for 20 min. After the incubation period, the reaction mixture containing Rh123 was removed, and the cells were washed three times with HBSS (Hank's Balanced Salt Solution) to remove any excess dye. The imaging was conducted under a blue light exciting filter using a microscope (Leica DMi8 microscope from Wetzlar, Germany). The resultant fluorescence emitted by Rh123 was observed in the green channel. The intensity of the green fluorescence is directly correlated with the mitochondrial membrane potential (MMP). Higher green fluorescence indicated a greater MMP, while lower fluorescence indicated a decrease in MMP.

2.10. NO assay by imaging DAR-2 fluorescence

Intracellular NO was determined by imaging a rhodamine-based live cell-permeable fluorescent probe DAR-2 that reacted explicitly with NO and generated intense fluorescence in the infra-red region (Kojima et al., 2001; Von Bohlen und Halbach, 2003). Cells were treated with respective agents for 24 h in a 12-well plate and labeled with DAR-2 at a final concentration of 10 µM for 2 h at the end of treatment. Then, cells were carefully washed with cold HBSS three times, and imaging was conducted using an appropriate filter in a microscope (Leica DMi8, Wetzlar, Germany). NO was also indirectly quantified by measuring nitrite liberated in cell culture media using Griess reagent at 540 nm in a plate reader (Synergy HT, Bio-Tek, Winooski, VT, USA). A standard of sodium nitrite (1–100 µM) prepared in culture media was similarly run for calculating purposes (Akhtar et al., 2022). Data are presented as % age of NO concentration in untreated control cells.

2.11. Protein estimation

The total protein content of the sample was determined using the BCA Protein Assay Kit from Sigma-Aldrich (MO, USA), following the provided instructions. The kit offers a convenient and reliable method for quantifying protein concentration in a sample.

2.12. Statistics

ANOVA (one-way analysis of variance) followed by Dunnett's multiple comparison tests were employed for the statistical analysis of the results. A burst of images was captured in specific experiments with constant exposure time, gain, saturation, and gamma. Corrected total cellular fluorescence (CTCF) was calculated using the ImageJ software (NIH, Bethesda, MD). To ensure consistency, the region of interest (ROI) manager command was used to restore a reasonably constant area for all images within an ImageJ session by utilizing the 'restore selection' command. CTCF was calculated by subtracting the mean background fluorescence (without cells) from the mean cellular fluorescence (i.e., mean integrated density). The image's scale bar was set using ImageJ, adjusting it in terms of pixels/micron, and then saving all images in JPEG format. Representative images from three independent experiments ($n = 3$) are shown for the specific experimental group captured by the Leica DFC450 camera from Germany. The data presented are the mean ± SD of three identical experiments ($n = 3$) conducted in triplicates for all biochemical and imaging experiments. Statistical significance was determined at $p < 0.05$.

3. Results

3.1. Mo NPs physicochemical properties

The transmission electron microscopy (TEM) analysis revealed that the size of the NPs was well below 100 nm, as indicated by the information provided by the supplier. Specifically, the average particle size was 37 ± 15 nm (Fig. 1 A). Furthermore, the shape of the Mo NPs was predominantly spherical (refer to Fig. 1 B). The energy-dispersive X-ray spectroscopy (EDS) results, shown in Fig. 1 C, indicated the absence of any other significant elemental presence. Table 1 summarizes the physicochemical properties of naïve Mo NPs and their adsorption behavior with BSA protein in aqueous media.

3.2. Mo NPs were highly biocompatible in HUVE cells, enhancing cellular antioxidant GSH

Mo NPs have shown minimal cytotoxicity and excellent biocompatibility, making them suitable for biomedical applications, as revealed by MTT assay and phase-contrast imaging in Fig. 2A and 2B, respectively. Furthermore, Mo NPs have the potential to enhance the antioxidant defense system within cells (2B), as evidenced by their capacity to increase GSH levels by 128 ± 4.9 % in cells treated with 100 µg/mL of Mo NPs in comparison to untreated control cells. GSH enhancement by Mo NPs was high at 100 µg/mL. Therefore, this concentration was chosen to advance study in subsequent modulatory experiments in the presence of Mo NPs against oxidative stress inducers.

3.3. Mo NPs significantly protected cells from exogenous oxidant t-BHP and H_2O_2

Mo NPs have demonstrated their ability to protect cells from exogenous oxidants, such as t-BHP and H_2O_2, as depicted in Fig. 3. Data suggests Mo NPs to be significantly preventive against the two oxidants. The study on cell viability showed that applying Mo NPs resulted in an increase of 71 % and 69 %, respectively, for what would be 50 % against the IC50 of t-BHP and H_2O_2. While the indirect method of assessing cell viability by MTT assay has little capacity to differentiate the mechanism of toxicity caused by t-BHP from that induced by H_2O_2, phase-contrast, and CalceinAM fluorescence images revealed a significant difference in morphology of damaged cells induced by t-BHP and H_2O_2 treatments (see cell images in Fig. 3A). T-BHP-treated cells exhibited more adherent properties and much weaker CalceinAM fluorescence than H2O2-treated cells, where damaged cells were mainly blown away from the substratum with minimal effect on live-dye CalceinAM fluorescence. Exposure

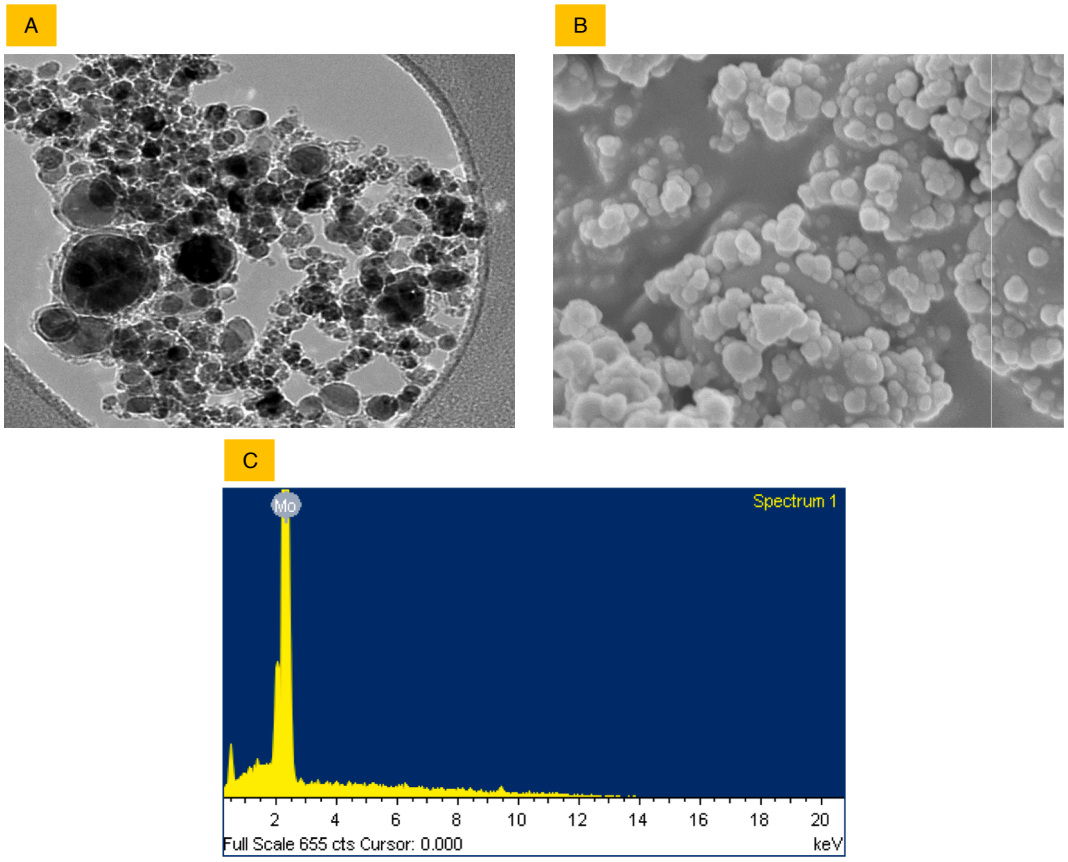

Fig. 1. Characterization of Mo NPs in terms of size and shape was conducted using TEM (A) and SEM (B), respectively. The chemical composition was confirmed through EDS (C) measurements.

Table 1
Physicochemical properties of Mo NPs and its adsorption behaviour with BSA protein in aqueous media.

Physicochemical Properties	
TEM size	37 ± 15 nm
SEM shape	Spherical
EDS analysis	Not detectable
BSA adsorption properties	
BSA adsorption in pure water	11 ± 1.5 %
BSA adsorption in culture media	8.5 ± 1.3 %

to IC50s of both oxidants leads to 50 % cell death assayed by MTT, but CalceinAM fluorescence is much weaker in t-BHP-treated cells than in H_2O_2-treated cells. Even treatment of Mo NPs did not cause recovery of lost CalceinAM fluorescence from the cells that received co-exposure to Mo NPs plus IC50 of t-BHP.

3.4. Mo NPs significantly restored the loss of mitochondrial membrane potential and caused decreases in ROS against exogenous oxidant exposure

Mo NPs effectively restored the mitochondrial membrane potential lost against exogenous oxidants, promoting the normal functioning of mitochondria (Fig. 4A and B). The study's findings on MMP revealed that the application of Mo NPs with oxidants has resulted in a substantial increase in the gain of MMP. Specifically, the gain of MMP has increased to 74 % and 73 %, respectively, which is significantly higher than the MMP observed at t-BHP and H_2O_2, which would otherwise reduce to 63 % and 48 %, respectively. In addition, it has been observed that Mo NPs significantly reduce the levels of reactive oxygen species (ROS) that are typically elevated due to exposure to oxidants. Although Mo NPs significantly elevated $O_2^{\bullet-}$ in HUVE cells as measured by the DHE probe (Fig. 4A and C), this increase in ROS did not translate into any adverse effect in terms of MMP. Moreover, Mo NPs significantly mitigated ROS, which appeared to increase with the oxidant treatments (Fig. 4D).

3.5. NO concentration was raised significantly higher in cells under the lethal concentration of t-BHP as compared to the non-lethal concentration of t-BHP

Given the involvement of Mo in the NO metabolism and the dependency of HUVE cells on NO signaling for crucial functions, we measured the levels of NO by NO-specific cell-permeant DAR-2 fluorescent dye (5A and B) and the Griess assay (Fig. 5C). Our results show that NO was not produced significantly by Mo NPs alone or by t-BHP or H_2O_2. However, NO generation was significantly high when HUVE cells were co-exposed with Mo NPs and oxidants. The study's results indicate that the presence of Mo NPs significantly enhances NO induction in cells. Treatment with IC50 of t-BHP alone resulted in a 1.7-fold increase in NO production while adding Mo NPs led to a substantial increase of over 6-fold. Similarly, the IC50 of H_2O_2 caused a 1.3-fold induction of NO alone, which was further increased to 2.5-fold in the presence of Mo NPs. These findings suggest that Mo NPs may have a synergistic effect on the production of NO in cells under oxidant exposure. Further research is needed to fully understand this effect's mechanisms and investigate potential therapeutic applications. Overall, these results highlight the potential of Mo NPs as a promising tool for enhancing cellular responses and improving health outcomes.

4. Discussion

Mo NPs belong to a group of catalytically active NPs that play a

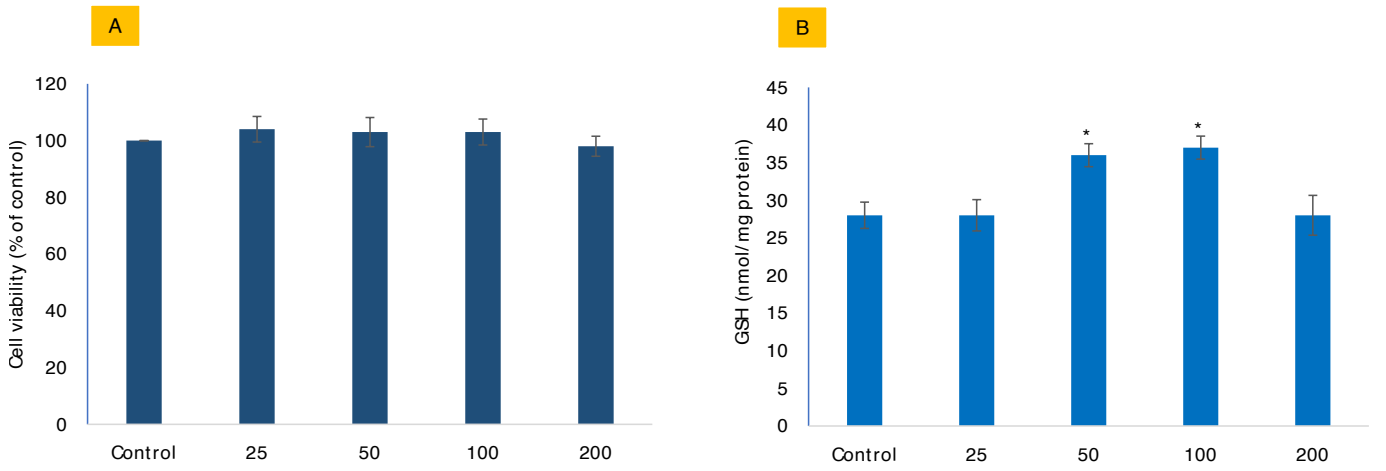

Fig. 2. The potential biocompatibility of Mo NPs in HUVE cells was assessed by evaluating cell viability (A) using the MTT bioassay and intracellular GSH levels (B) in response to varying concentrations of Mo NPs. The concentrations are expressed in μg/mL. The data represents the mean ± SD of three identical experiments (n = 3) in triplicates. * Denotes statistically significant differences compared to the control ($p < 0.05$).

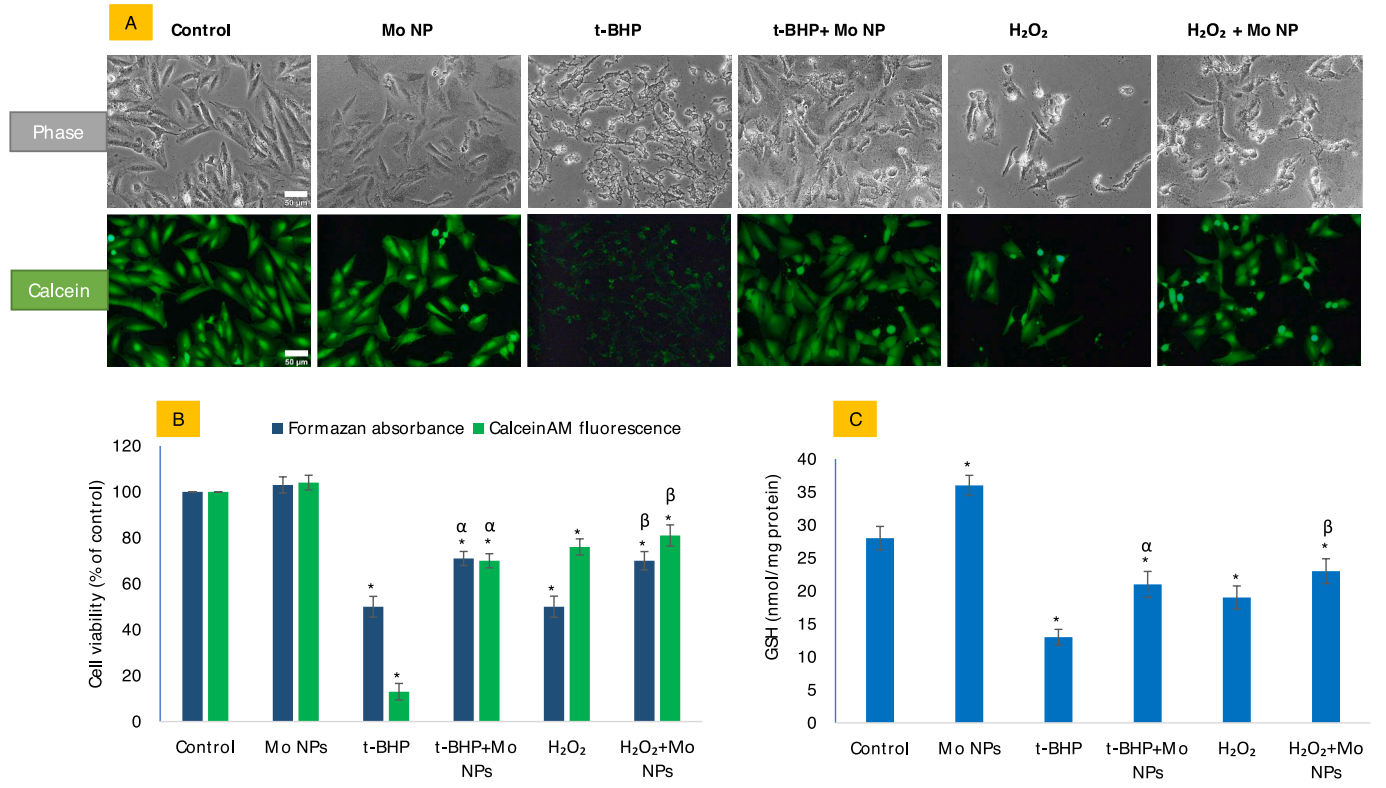

Fig. 3. The potential antioxidative properties of Mo NPs in HUVE cells were investigated concerning the IC50 values of two oxidants: t-BHP) and H_2O_2. In this study, Mo NPs refer to a concentration of 100 μg/mL of Mo NPs, while t-BHP and H_2O_2 represent the IC50 values of t-BHP and H_2O_2, respectively, as indicated in all subsequent figures. Figure (A) displays phase-contrast images (upper panel labeled as 'phase') and calceinAM green images (lower panel labeled as 'calcein') that were captured for the same set of treatments described above the images. The intensity of calceinAM fluorescence is compared with the MTT bioassay in Figure (B). Figure (C) summarizes the potential antioxidative effect of Mo NPs on intracellular GSH levels against the two oxidants tested in this study. The scale bar, present only in the control images, represents a length of 50 μm captured by a 20 × objective. The data presented in this study are the mean ± standard deviation of three identical experiments (n = 3) conducted in triplicate. * denotes statistically significant differences compared to the control ($p < 0.05$). The symbols α and β denote a significant difference in the response of Mo NPs (100 μg/mL) alone versus co-exposure with t-BHP or H_2O_2, respectively. (For interpretation of the references to color in this figure legend, the reader is referred to the web version of this article.)

crucial role in modulating reactive oxygen species (ROS), including the generation of deleterious hydroxide radicals (Ni et al., 2018). These NPs are involved in the intricate dynamics of antioxidative and oxidative phases within cells (Ni et al., 2018). In our study, we investigated the adsorption of Mo NPs (37 ± 15 nm) with BSA protein. The results suggest that the NPs have a low affinity for proteins, as they adsorb only a tiny amount compared to that reported for the NPs of CeO_2 and yttrium oxide article (Akhtar et al., 2020). The primary surface of NPs may undergo significant changes due to the high adsorption of molecules or ions. This may result in a secondary surface with different properties and interactions than the original one (Liu et al., 2021). The secondary surface may not reflect the primary chemical composition of NPs, which

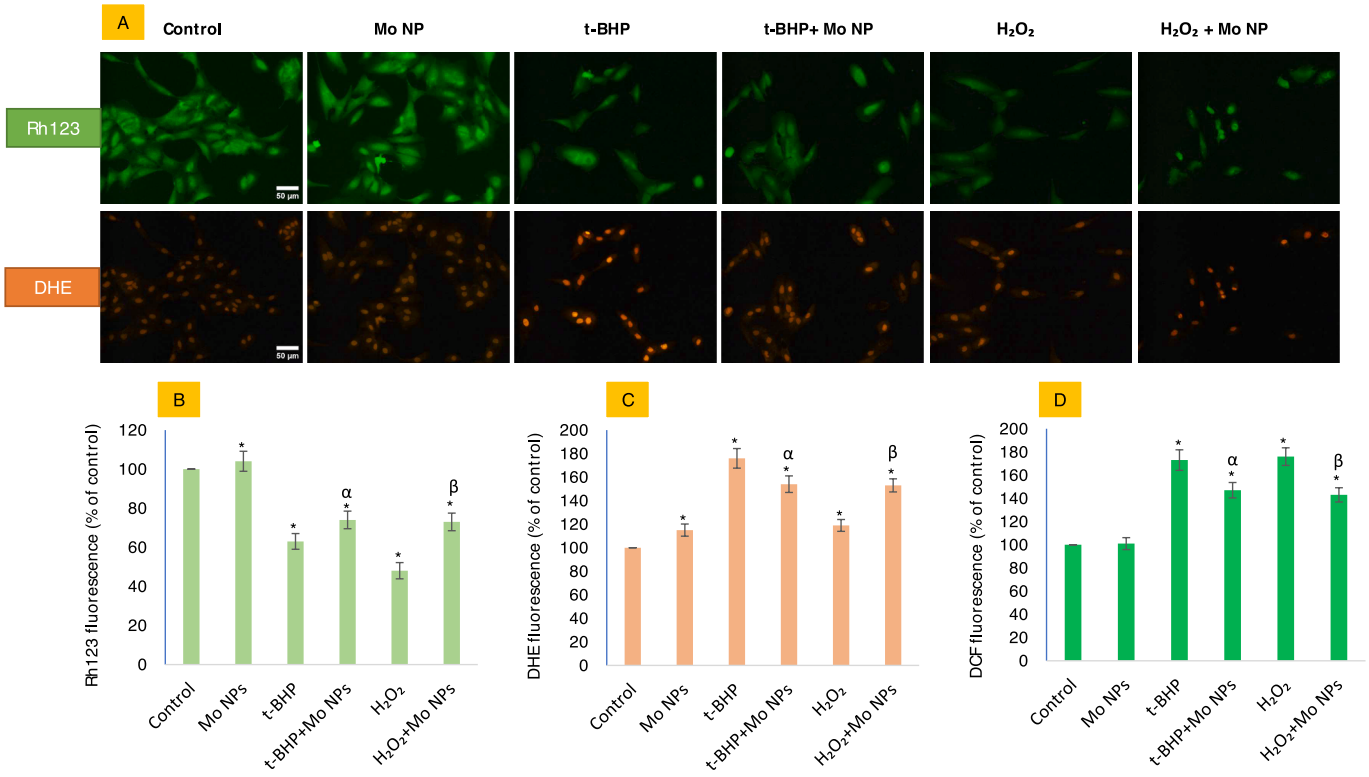

Fig. 4. Mitochondrial membrane potential (MMP) and superoxide radical ($O_2^{\bullet-}$) in HUVE cells were determined by live cell imaging co-labeled with two probes. The evaluation of MMP was conducted using the Rh123 probe, as shown in the upper green images in Fig. 4A, and the production of $O_2^{\bullet-}$ with the $O_2^{\bullet-}$-specific DHE probe, as depicted in the red fluorescing images in Fig. 4A (lower panel). The corresponding fluorescence intensities can be found in Figures (B) and (C), respectively. General ROS levels were assessed using DCFH-DA (D). The fluorescence intensities of individual cells in each treatment group were quantified using the ImageJ software provided by NIH, Bethesda, US. The scale bar, present only in the control images, represents a length of 50 μm captured by a 20 × objective. The data presented in this study are the mean ± standard deviation of three identical experiments (n = 3) conducted in triplicate. * denotes statistically significant differences compared to the control ($p < 0.05$). The symbols α and β denote a significant difference in the response of Mo NPs (100 μg/mL) alone versus co-exposure with t-BHP or H_2O_2, respectively. (For interpretation of the references to color in this figure legend, the reader is referred to the web version of this article.)

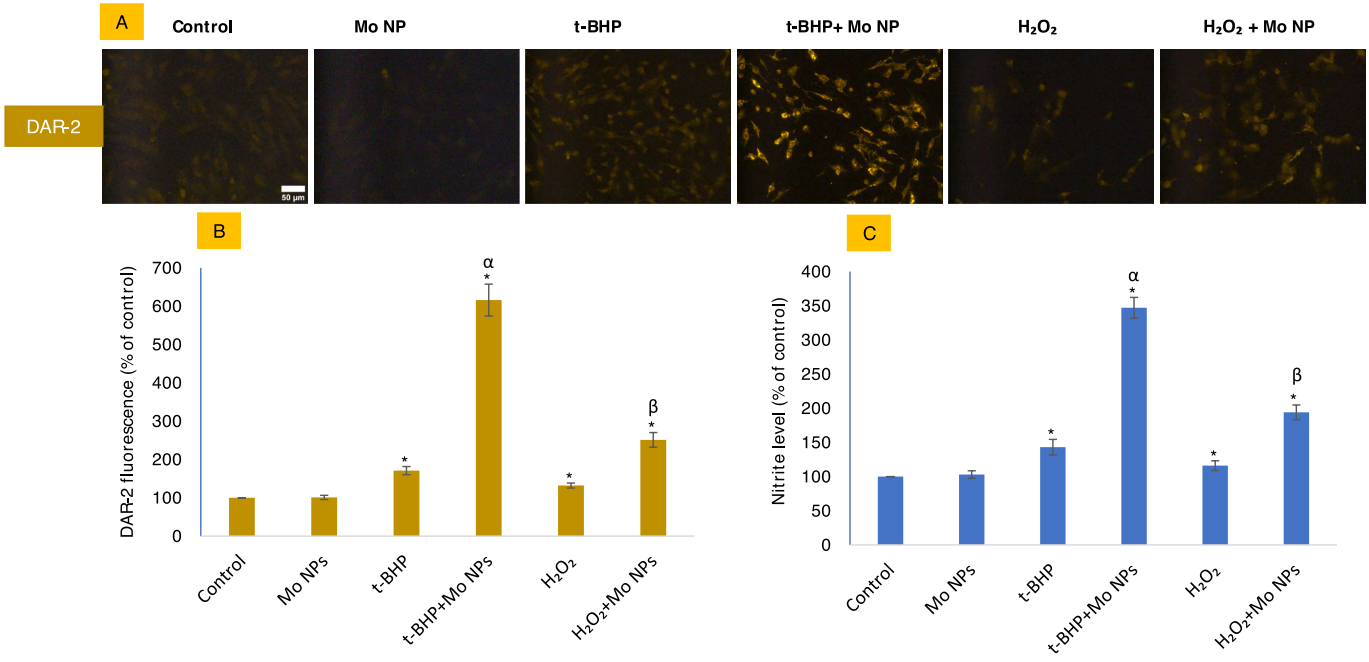

Fig. 5. NO levels were measured by imaging live cells labeled with NO-specific DAR-2 probe as given in figures (A and B). NO was also indirectly analyzed by Griess reagent (C). The scale bar, present only in the control images, represents a length of 50 μm captured by a 20 × objective. The data presented in this study are the mean ± standard deviation of three identical experiments (n = 3) conducted in triplicate. * denotes statistically significant differences compared to the control ($p < 0.05$). The symbols α and β denote a significant difference in the response of Mo NPs (100 μg/mL) alone versus co-exposure with t-BHP or H_2O_2, respectively.

may affect their applications and effects (Liu et al., 2021; Ni et al., 2018). The finding in this study implies that Mo NPs remain with naïve surface properties in the complete culture media that would be of great significance in terms of control and reproducibility. The biocompatibility of Mo NPs was demonstrated in HUVE cells. No significant cytotoxic effects were observed in HUVE cells for the NPs of Mo. Overall, the high biocompatibility of Mo NPs in HUVE cells highlights their potential for further development and exploration in biomedical research and applications. Moreover, Mo NPs positively affect cellular antioxidant status, as seen from the cellular GSH replenishment. Antioxidant GSH is a ubiquitous non-enzymatic molecule that protects cells from damage caused by harmful ROS/RNS actions. This promoted antioxidant capacity, as evidenced by the increase in GSH level in NP-treated cells, which allows cells to tolerate induced toxicity that exogenous oxidants and other toxic insults might cause. In addition, Mo NPs enhance the cellular antioxidant status, as indicated by the increase in cellular GSH in cells treated with Mo NPs. Recall that GSH is a ubiquitous non-enzymatic antioxidant that protects cells from the damage caused by the harmful effects of oxidative reactions (Deng et al., 2018).

Oxidants t-BHP and H_2O_2 are potent oxidative stress inducers commonly used in cellular and molecular studies to mimic oxidative damage. The distinction in morphological effects and CalceinAM fluorescence observed by t-BHP and H_2O_2 treatments in HUVE cells lead to differential disruptions between cells and culture substratum. They can be an exciting topic for further research (Bergamini et al., 2023). A possible implication of this study is that t-BHP and H_2O_2 may trigger distinct pathways, resulting in different mechanisms of cell detachments as an alternative method to investigate cell-material interaction and biocompatibility in a recent study (Bergamini et al., 2023). The loss of mitochondrial membrane potential (MMP) due to ROS-induced leakages in the mitochondrial membrane is often associated with the commencement of cell death programs. Cellular energy is conserved as protons (H^+ ions) in intermembrane space by pumping mitochondrial complexes I, III, and IV against an electrochemical gradient. ATP is synthesized when protons move into the matrix down the gradient (Mitchell, 1966; Zorova et al., 2018). Loss of MMP indicates energy stress that can be followed by releasing death-inducing factors in the cytosol (Zorova et al., 2018). Data on MMP and ROS in this study suggests that a controlled level of induced ROS can be advantageous, as it prepares cells to combat induced oxidative stress effectively. This is supported by the ability of Mo NPs to reduce ROS production and significantly restore lost mitochondrial membrane potential (MMP) in the presence of exogenous oxidants. This restoration is crucial for maintaining proper cellular metabolism and energy production (Zorova et al., 2018). By doing so, Mo NPs could have partially alleviated the stress placed on cells by exogenous oxidants.

Mo is a transition metal like iron and copper and is present in many redox enzymes of eukaryotes and prokaryotes dealing with NO metabolism (Mendel and Bittner, 2006). A limited repertoire of Mo-containing enzymes that deal with NO metabolism is present in mammalian cells, too (Valko et al., 2016). Oxidants have been known as strong modulators of NO signaling that can either activate or inhibit NO production via nitric oxide synthases (NOSs) or via non-NOS pathways that require enzymes with Mo as co-factors (DeMartino et al., 2019; Kim-Shapiro and Gladwin, 2014). Our results showed that Mo NPs did not affect NO production in HUVECs when exposed alone, suggesting that Mo NPs are incapable of inducing detectable levels of NO on their own and, hence, are not expected to interfere with NO signaling pathways. However, co-exposure of HUVECs to Mo NPs and oxidants significantly increased NO production·H_2O_2 has been found to stimulate the production of NO in endothelial cells by activating the transcription of the enzyme endothelial NOS (eNOS) (Thomas et al., 2007). This process can result in increased levels of NO, which has various beneficial effects on cellular health. However, when exposed to high concentrations of H_2O_2, eNOS can become "uncoupled." This means that instead of synthesizing NO, it produces the $O_2^{\bullet-}$ radical. $O_2^{\bullet-}$ can cause oxidative damage to cellular machinery and disrupt normal cellular function. Therefore, high levels of H_2O_2 can be detrimental to cells. Similarly, t-BHP has been reported to increase NO production in human retinal pigment epithelial cells treated with 200 μM of t-BHP over a range of 16- to 20 h (Sripathi et al., 2012). It is important to note that NO production by NOS depends on oxygen availability (O_2). However, it is also possible for NO to be generated through alternative pathways that are not dependent on NOSs and oxygen availability. One such pathway involves the serial reduction of inorganic nitrate and nitrite to NO (DeMartino et al., 2019; Kim-Shapiro and Gladwin, 2014).

The enhanced generation of NO can be attributed to the unique properties and characteristics of both t-BHP and Mo NPs. t-BHP is a potent oxidizing agent that could readily undergo decomposition in the presence of catalysts or nanomaterials, such as Mo NPs. Compared to H_2O_2, t-BHP may produce a greater NO yield due to its higher oxidation potential. This enhanced reactivity of t-BHP, in combination with Mo NPs, is a favorable choice for applications that require high concentrations of NO, as in biomedical research. The generation of NO triggered by H_2O_2 was noteworthy only when exposed to cytotoxic concentrations of H_2O_2 in the presence of Mo NPs (Mo NPs). In contrast, t-BHP caused significant NO generation even at non-cytotoxic concentrations (data not shown), although it was less than that caused by the cytotoxic concentration of t-BHP. In summary, H_2O_2 and t-BHP can influence NO production in cells. Moreover, the simultaneous presence of NO and oxidants can make reactions yield more deleterious reactive nitrogen species (RNS), such as peroxynitrite (Radi, 2013). High NO in the presence of $O_2^{\bullet-}$ can induce lipid peroxidation, leading to disintegrity in membrane structures (Farah et al., 2018). $ONOO^-$ can create a favorable environment for nitration (addition of a $–NO_2$ group to organic molecules) and can oxidize crucial thiols like H_2O_2 (Radi, 2018), resulting in the phenomenon of 'nitrative' and 'nitrosative' stress that denotes the alteration in activities of proteins and enzymes due to nitration (addition of $–NO_2$ moiety) and nitrosation (addition of –NO moiety) respectively. These actions can significantly inhibit or alter the activity of many proteins and might have considerable implications (Radi, 2018). For example, human mitochondrial MnSOD is inhibited by $ONOO^-$ (self)-mediated nitration (of Tyr34 of hMnSOD), resulting in the inhibition of the enzyme (DeMartino et al., 2019; Kim-Shapiro and Gladwin, 2014). Moreover, $ONOO^-$ can generate powerful one-electron oxidants after reacting with CO_2 at 1–2 mM concentrations in active cells. Nitrative and nitrosative stresses are, therefore, considered the hallmark of high NO production (DeMartino et al., 2019; Heinrich et al., 2013; Kim-Shapiro and Gladwin, 2014) as oxidative stress is the hallmark of increased ROS or decreased antioxidants or both.

5. Conclusion

Findings in this report suggest that Mo NPs may have a synergistic effect on the production of NO in cells under oxidant exposure. High production of NO in the presence of Mo NPs can abruptly limit the reactive oxygen scavenging capacity of Mo NPs. This finding also suggests that NO modulatory strategies can potentially impact fine-tuning the antioxidative properties of Mo-based NPs. This implies that modulating NO levels could enhance the antioxidative activity of Mo-based NPs/agents. The combination of t-BHP and Mo NPs demonstrates a novel and powerful system of generating NO inside cells. As NO-generating systems are rare compared to ROS-generating systems, this finding may have significant implications in biomedical research, where NO-controlled production is desired.

CRediT authorship contribution statement

Mohd Javed Akhtar: Writing – review & editing, Writing – original draft, Visualization, Investigation, Funding acquisition, Conceptualization. **Maqusood Ahamed:** Conceptualization, Supervision, Writing – review & editing. **Sudhir Kumar:** Writing – original draft, Supervision,

Data curation, Conceptualization. **Rashid Lateef:** Visualization, Software, Methodology. **Zabn Alaizeri:** Project administration, Methodology, Formal analysis. **Hisham Alhadlaq:** Resources, Data curation. **Pavan Rajanahalli:** Writing – original draft, Supervision.

Declaration of competing interest

The authors declare that they have no known competing financial interests or personal relationships that could have appeared to influence the work reported in this paper.

Acknowledgments

The authors acknowledge the Research Institute/Centre supporting program (RICSP-24-1), King Saud University, Riyadh, Saudi Arabia.

Appendix A. Supplementary material

Supplementary data to this article can be found online at https://doi.org/10.1016/j.jksus.2024.103525.

Data availability

Data will be made available on request.

References

Ahmed, J., Majeed Khan, M.A., Alshehri, S.M., 2021. Zinc molybdenum oxide submicron plates as electro-catalysts for hydrogen evolution reactions in acidic medium. Mater. Lett. 284, 128996. https://doi.org/10.1016/j.matlet.2020.128996.

Akhtar, M.J., Ahamed, M., Alrokayan, S.A., Ramamoorthy, M.M., Alaizeri, Z.A.M., 2020. High surface reactivity and biocompatibility of Y2O3 NPs in human MCF-7 epithelial and HT-1080 fibro blast cells. Molecules 25. https://doi.org/10.3390/molecules25051137.

Akhtar, M.J., Ahamed, M., Alhadlaq, H., 2021. Anti-inflammatory ceo2 nanoparticles prevented cytotoxicity due to exogenous nitric oxide donors via induction rather than inhibition of superoxide/nitric oxide in huve cells. Molecules 26. https://doi.org/10.3390/molecules26175416.

Akhtar, M.J., Ahamed, M., Alhadlaq, H., 2022. CeO2-Zn Nanocomposite Induced Superoxide, Autophagy and a Non-Apoptotic Mode of Cell Death in Human Umbilical-Vein-Derived Endothelial (HUVE) Cells. Toxics 10, 250. https://doi.org/10.3390/toxics10050250.

Akhtar, M.J., Ahamed, M., Alhadlaq, H., 2023. Bismuth Oxide (Bi2O3) Nanoparticles Cause Selective Toxicity in a Human Endothelial (HUVE) Cell Line Compared to Epithelial Cells. Toxics 11. https://doi.org/10.3390/toxics11040343.

Baracca, A., Sgarbi, G., Solaini, G., Lenaz, G., 2003. Rhodamine 123 as a probe of mitochondrial membrane potential: Evaluation of proton flux through F0 during ATP synthesis. Biochim. Biophys. Acta - Bioenerg. 1606, 137–146. https://doi.org/10.1016/S0005-2728(03)00110-5.

Bergamini, V., Resca, E., Portone, A., Petrachi, T., Ganzerli, F., Truzzi, S., Mari, G., Rovati, L., Dominici, M., Veronesi, E., 2023. Label-Free Optical Sensing and Medical Grade Resins: An Advanced Approach to Investigate Cell–Material Interaction and Biocompatibility. Pharm. 2023, Vol. 15, Page 2043 15, 2043. Doi: 10.3390/PHARMACEUTICS15082043.

Bohlen, V., Halbach, O., 2003. Nitric oxide imaging in living neuronal tissues using fluorescent probes. Nitric Oxide - Biol. Chem. 9, 217–228. https://doi.org/10.1016/j.niox.2004.01.001.

DeMartino, A.W., Kim-Shapiro, D.B., Patel, R.P., Gladwin, M.T., 2019. Nitrite and nitrate chemical biology and signalling. Br. J. Pharmacol. https://doi.org/10.1111/bph.14484.

Deng, Y., Jia, F., Chen, S., Shen, Z., Jin, Q., Fu, G., Ji, J., 2018. Nitric oxide as an all-rounder for enhanced photodynamic therapy: Hypoxia relief, glutathione depletion and reactive nitrogen species generation. Biomaterials 187, 55–65. https://doi.org/10.1016/j.biomaterials.2018.09.043.

Dhas, N., Kudarha, R., Garkal, A., Ghate, V., Sharma, S., Panzade, P., Khot, S., Chaudhari, P., Singh, A., Paryani, M., Lewis, S., Garg, N., Singh, N., Bangar, P., Mehta, T., 2021. Molybdenum-based hetero-nanocomposites for cancer therapy, diagnosis and biosensing application: Current advancement and future breakthroughs. J. Control. Release. https://doi.org/10.1016/j.jconrel.2020.12.015.

Eremin, A.V., Gurentsov, E.V., Kolotushkin, R.N., Musikhin, S.A., 2018. Room-temperature synthesis and characterization of carbon-encapsulated molybdenum nanoparticles. Mater. Res. Bull. 103, 186–196. https://doi.org/10.1016/j.materresbull.2018.03.026.

Farah, C., Michel, L.Y.M., Balligand, J.L., 2018. Nitric oxide signalling in cardiovascular health and disease. Nat. Rev. Cardiol. https://doi.org/10.1038/nrcardio.2017.224.

Feng, P., Cao, W., 2016. Properties, Application and Synthesis Methods of Nano-Molybdenum Powder. J. Mater. Sci. Chem. Eng. 04, 36–44. https://doi.org/10.4236/msce.2016.49004.

Fridovich, I., 2003. With the help of giants. Annu. Rev. Biochem. https://doi.org/10.1146/annurev.biochem.72.081902.140918.

Han, R., Xiao, Y., Bai, Q., Choi, C.H.J., 2022. Self-therapeutic metal-based nanoparticles for treating inflammatory diseases. Acta Pharm. Sin. b. https://doi.org/10.1016/j.apsb.2022.07.009.

Heinrich, T.A., Da Silva, R.S., Miranda, K.M., Switzer, C.H., Wink, D.A., Fukuto, J.M., 2013. Biological nitric oxide signalling: Chemistry and terminology. Br. J. Pharmacol. https://doi.org/10.1111/bph.12217.

Hissin, P.J., Hilf, R., 1976. A fluorometric method for determination of oxidized and reduced glutathione in tissues. Anal. Biochem. 74, 214–226. https://doi.org/10.1016/0003-2697(76)90326-2.

Johnson, L.V., Walsh, M.L., Chen, L.B., 1980. Localization of mitochondria in living cells with rhodamine 123. Proc. Natl. Acad. Sci. u. s. a. 77, 990–994. https://doi.org/10.1073/pnas.77.2.990.

Kashyap, B.K., Singh, V.V., Solanki, M.K., Kumar, A., Ruokolainen, J., Kesari, K.K., 2022. Smart Nanomaterials in Cancer Theranostics: Challenges and Opportunities. ACS Omega. https://doi.org/10.1021/acsomega.2c07840.

Khafaji, M., Zamani, M., Golizadeh, M., Bavi, O., 2019. Inorganic nanomaterials for chemo/photothermal therapy: a promising horizon on effective cancer treatment. Biophys. Rev. 11, 335–352. https://doi.org/10.1007/S12551-019-00532-3.

Kim-Shapiro, D.B., Gladwin, M.T., 2014. Mechanisms of nitrite bioactivation. Nitric Oxide - Biol. Chem. Doi: 10.1016/j.niox.2013.11.002.

Kojima, H., Hirotani, M., Nakatsubo, N., Kikuchi, K., Urano, Y., Higuchi, T., Hirata, Y., Nagano, T., 2001. Bioimaging of nitric oxide with fluorescent indicators based on the rhodamine chromophore. Anal. Chem. 73, 1967–1973. https://doi.org/10.1021/ac001136i.

Liu, Y., Wang, J., Xiong, Q., Hornburg, D., Tao, W., Farokhzad, O.C., 2021. Nano-Bio Interactions in Cancer: From Therapeutics Delivery to Early Detection. Acc. Chem. Res. 54, 291–301. https://doi.org/10.1021/acs.accounts.0c00413.

Mendel, R.R., Bittner, F., 2006. Cell biology of molybdenum. Biochim. Biophys. Acta - Mol. Cell Res. Doi: 10.1016/j.bbamcr.2006.03.013.

Mitchell, P., 1966. Chemiosmotic coupling in oxidative and photosynthetic phosphorylation. Biol. Rev. Camb. Philos. Soc. https://doi.org/10.1111/j.1469-185x.1966.tb01501.x.

Mosmann, T., 1983. Rapid colorimetric assay for cellular growth and survival: Application to proliferation and cytotoxicity assays. J. Immunol. Methods 65, 55–63. https://doi.org/10.1016/0022-1759(83)90303-4.

Neri, S., Mariani, E., Meneghetti, A., Cattini, L., Facchini, A., 2001. Calcein-acetyoxymethyl cytotoxicity assay: Standardization of a method allowing additional analyses on recovered effector cells and supernatants. Clin. Diagn. Lab. Immunol. 8, 1131–1135. https://doi.org/10.1128/CDLI.8.6.1131-1135.2001.

Ni, D., Jiang, D., Kutyreff, C.J., Lai, J., Yan, Y., Barnhart, T.E., Yu, B., Im, H.J., Kang, L., Cho, S.Y., Liu, Z., Huang, P., Engle, J.W., Cai, W., 2018. Molybdenum-based nanoclusters act as antioxidants and ameliorate acute kidney injury in mice. Nat. Commun. 9, 1–11. https://doi.org/10.1038/s41467-018-07890-8.

Radi, R., 2013. Peroxynitrite, a stealthy biological oxidant. J. Biol. Chem. https://doi.org/10.1074/jbc.R113.472936.

Radi, R., 2018. Oxygen radicals, nitric oxide, and peroxynitrite: Redox pathways in molecular medicine. Proc. Natl. Acad. Sci. U. S. A. 115, 5839–5848. https://doi.org/10.1073/pnas.1804932115.

Ren, X., Chen, D., Wang, Y., Li, H., Zhang, Y., Chen, H., Li, X., Huo, M., 2022. Nanozymes-recent development and biomedical applications. J. Nanobiotechnology. https://doi.org/10.1186/s12951-022-01295-y.

Reuter, S., Gupta, S.C., Chaturvedi, M.M., Aggarwal, B.B., 2010. Oxidative stress, inflammation, and cancer: How are they linked? Free Radic. Biol. Med. https://doi.org/10.1016/j.freeradbiomed.2010.09.006.

Sripathi, S.R., He, W., Um, J.-Y., Moser, T., Dehnbostel, S., Kindt, K., Goldman, J., Frost, M.C., Jahng, W.J., 2012. Nitric oxide leads to cytoskeletal reorganization in the retinal pigment epithelium under oxidative stress. Adv. Biosci. Biotechnol. 03, 1167–1178. https://doi.org/10.4236/abb.2012.38143.

Thomas, S., Kotamraju, S., Zielonka, J., Harder, D.R., Kalyanaraman, B., 2007. Hydrogen peroxide induces nitric oxide and proteosome activity in endothelial cells: A bell-shaped signaling response. Free Radic. Biol. Med. 42, 1049–1061. https://doi.org/10.1016/j.freeradbiomed.2007.01.005.

Valko, M., Jomova, K., Rhodes, C.J., Kuča, K., Musílek, K., 2016. Redox- and non-redox-metal-induced formation of free radicals and their role in human disease. Arch. Toxicol. https://doi.org/10.1007/s00204-015-1579-5.

Wang, H., Joseph, J.A., 1999. Quantifying cellular oxidative stress by dichlorofluorescein assay using microplate reader. Free Radic. Biol. Med. 27, 612–616. https://doi.org/10.1016/S0891-5849(99)00107-0.

Yang, H., Guo, Y., Zhuang, Z., Zhong, H., Hu, C., Liu, Z., Guo, Z., 2019. Molybdenum oxide nano-dumplings with excellent stability for photothermal cancer therapy and as a controlled release hydrogel. New J. Chem. 43, 14281–14290. https://doi.org/10.1039/c9nj03088c.

Zapór, L., Chojnacka-Puchta, L., Sawicka, D., Miranowicz-Dzierzawska, K., Skowroń, J., 2022. Cytotoxic and pro-inflammatory effects of molybdenum and tungsten disulphide on human bronchial cells. Nanotechnol. Rev. 11, 1263–1272. https://doi.org/10.1515/ntrev-2022-0073.

Zorova, L.D., Popkov, V.A., Plotnikov, E.Y., Silachev, D.N., Pevzner, I.B., Jankauskas, S. S., Babenko, V.A., Zorov, S.D., Balakireva, A.V., Juhaszova, M., Sollott, S.J., Zorov, D.B., 2018. Mitochondrial membrane potential. Anal. Biochem. 552, 50–59. https://doi.org/10.1016/j.ab.2017.07.009.